Defective Graphene as a High-Capacity Anode Material for Na- and Ca-Ion Batteries

ARTICLE *in* ACS APPLIED MATERIALS & INTERFACES · JANUARY 2014

Impact Factor: 6.72 · DOI: 10.1021/am404788e · Source: PubMed

3 AUTHORS, INCLUDING:

Dibakar Datta
Stanford University
26 PUBLICATIONS **265** CITATIONS
SEE PROFILE

Junwen Li
Brown University
26 PUBLICATIONS **793** CITATIONS
SEE PROFILE

ACS APPLIED MATERIALS & INTERFACES

Research Article

www.acsami.org

Defective Graphene as a High-Capacity Anode Material for Na- and Ca-Ion Batteries

Dibakar Datta,[†] Junwen Li,[‡] and Vivek B. Shenoy*[,‡]

[†]School of Engineering, Brown University, Providence, Rhode Island 02912, United States

[‡]Department of Materials Science and Engineering, University of Pennsylvania, Philadelphia, Pennsylvania 19104, United States

ABSTRACT: Because of their abundance, sodium and calcium can be attractive in ion batteries for large-scale grid storage. However, many of the anode materials being pursued have limitations including volume expansion, lack of passivating films, and slow kinetics. Here, we investigate the adsorption of Na and Ca on graphene with divacancy and Stone–Wales defects in graphene. Our results show that although adsorption of Na and Ca is not possible on pristine graphene, enhanced adsorption is observed on defective graphene because of increased charge transfer between the adatoms and defects. We find that the capacity of graphene increases with the density of the defects. For the maximum possible divacancy defect densities, capacities of 1450 and 2900 mAh/g for Na- and Ca-ion batteries, respectively, can be achieved. For Stone–Wales defects, we find maximum capacities of 1071 and 2142 mAh/g for Na and Ca, respectively. Our results provide guidelines to create better high-capacity anode materials for Na- and Ca-ion batteries.

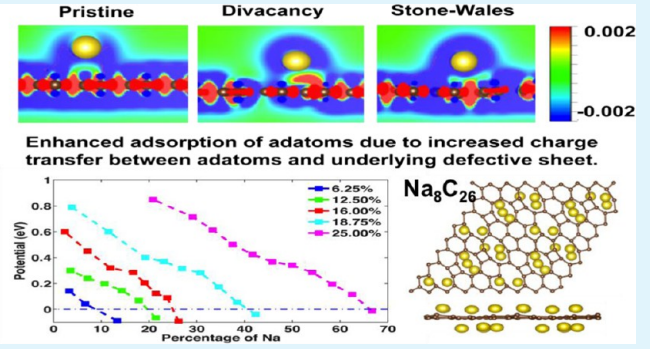

KEYWORDS: *defective graphene, Na ion, Ca ion, anode materials, batteries*

INTRODUCTION

Rechargable lithium-ion batteries (LIBs) have been extensively used in portable electronics, light vehicles, and miscellaneous power devices over the past decade.[1] In terms of energy density, the seemingly ubiquitous LIBs exhibit superb performance as compared to other types of rechargeable batteries.[2−5] However, among light metals, Li is a very rare element. Its concentration in the upper continental crust is estimated to be 35 ppm.[6] Hence, in recent years, there have been great concerns that available Li resources buried in the earth would not be sufficient to meet the ever increasing demands for LIBs.[7] These concerns have led to the active search for suitable alternatives.[8] Among these, sodium-ion batteries (NIBs)[8,9] and calcium-ion batteries (CIBs)[10,11] have drawn significant attention.

Although the energy density of a NIB is generally lower than that of a LIB,[7] high energy density becomes less critical for battery applications in large-scale storage.[9] More importantly, the abundance and low cost of Na in the earth (10 320 ppm in seawater and 28 300 ppm in the lithosphere)[12,13] and low reduction potential (−2.71 V vs standard hydrogen electrode (SHE)) provide a lucrative low-cost, safe, and environmentally benign alternative to Li in batteries.[14−16] Like NIBs, CIBs offer several benefits such as low cost, natural abundance, chemical safety, low reduction potential (−2.87 V vs SHE), and lighter mass-to-charge ratio.[11,17] The use of polyvalent cations is the key to obtaining much larger discharge capacities than those of LIBs.[10] Moreover, nature stores energy with Na and Ca ions, not Li ions.[18]

Electrochemical properties of the electrode materials are the cynosure of important battery-performance characteristics such as specific capacity and operating voltage.[9] Hence, the major challenge in advancing NIB and CIB technologies lies in finding better electrode materials. The best starting point is the investigation of the structure and chemistries of electrode materials that function well for Li intercalation. Graphite, the most widely used anode material for LIBs, has a relatively low gravimetric capacity. Even for NIBs and CIBs, use of graphite yields very low capacity.[19] Recent experimental studies show that if we can lower the dimensionality of the conventional anode materials via nanotechnology, we can achieve higher capacity. For example, low-dimensional materials, like graphene[20,21] and its oxide,[22] carbon nanotubes,[23,24] and silicon nanowires,[25] have been widely investigated as a possible replacement for graphite in LIBs.

Among the low-dimensional materials, graphene has attracted enormous attention since its discovery in 2004.[26] Besides its fascinating physical properties, it also shows considerable promise as atom/molecule containers for potential applications in electrochemical storage devices.[27−29] However, impurities and defects, both Stone–Wales (SW) and divacancy

Received: October 29, 2013
Accepted: January 13, 2014

   dx.doi.org/10.1021/am404788e | ACS Appl. Mater. Interfaces XXXX, XXX, XXX−XXX

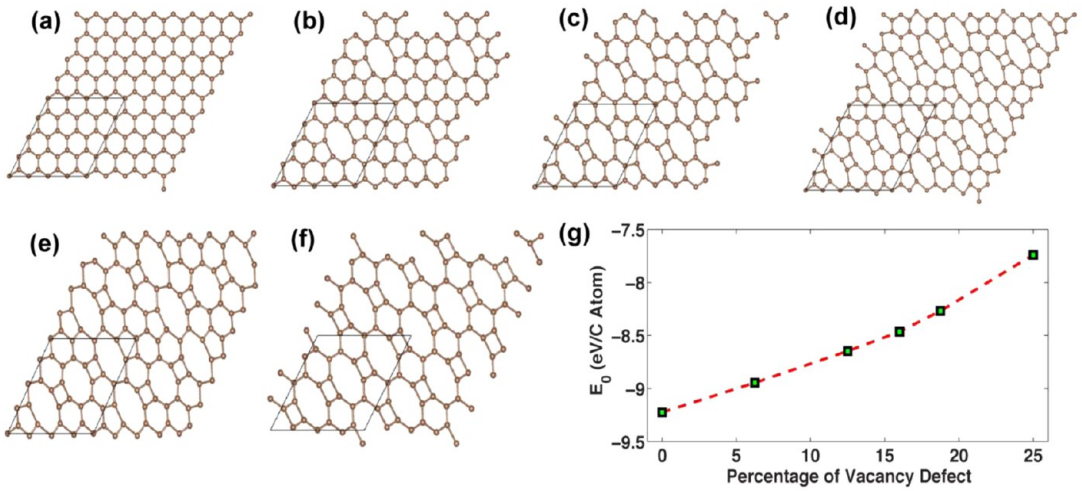

Figure 1. (a) Pristine graphene and graphene with DV defects: (b) 6.25, (c) 12.50, (d) 16.00, (e) 18.75, and (f) 25%. Systems shown here are 2 × 2 in size with periodicity in their in-plane dimensions. The super cell used in the calculation is marked in black. All systems are relaxed structure. (g) Equilibrium energy per carbon atom for different percentages of DV defect.

(DV), are always present in graphene.[30−32] Recent studies discovered several structural defects in graphene at an atomic resolution using transmission electron microscopy (TEM)[33,34] and scanning tunneling microscopy (STM).[35,36] Structural defects have a strong influence on the electronic, optical, thermal, and mechanical properties of graphene.[30] Recent DFT studies[37,38] predicted that the presence of defects would enhance the Li adsorption on graphene, giving a higher gravimetric capacity. Hence, the open question of how will defects in graphene influence the adsorption of Na and Ca remains. To answer this question in detail, we have carried out the first-principles calculations based on DFT to investigate thoroughly the Na and Ca adsorption on graphene with various percentages of DV and SW defects.

METHODOLOGY

All calculations were performed using the Vienna Ab initio Simulation Package (VASP)[39] with the projector augmented wave (PAW)[40,41] method and the Perdew−Burke−Ernzerhof (PBE)[42] form of the generalized gradient approximation (GGA) for exchange and correlation functional. An energy cutoff of 600 eV was used in the plane wave expansion of wave functions. The Brillouin zones of 4 × 4 and 5 × 5 super cell were sampled with Γ-centered *k*-point grids of 9 × 9 × 1 and 7 × 7 × 1, respectively. To avoid the spurious coupling effect between periodic graphene layers along the normal direction, the vacuum separation in the model structure was set to 18 Å. All atoms and super-cell lattice vectors are relaxed with a force tolerance of 0.02 eV/Å.

The potential, *V*, is defined as[43]

$$V = -\frac{\Delta G_f}{n} \tag{1}$$

where *n* is the number of X (X = Na, Ca) atoms inserted in the computational cell. The change in Gibb's free energy is

$$\Delta G_f = \Delta E_f + P\Delta V_f - T\Delta S_f \tag{2}$$

Because the term $P\Delta V_f$ is on the order of 10^{-5} eV[43] whereas the term $T\Delta S_f$ is on the order of the thermal energy (26 meV at room temperature), the entropy and the pressure terms can be neglected, and the free energy will be approximately equal to the formation energy, ΔE_f, obtained from DFT calculations. The formation energy is defined as

$$\Delta E_f = E_{X_nG} - (nE_X + E_G) \tag{3}$$

where E_{X_nG} is the total energy of the Na/Ca intercalated graphene, E_X is the total energy of a single Na/Ca atom in elemental bcc Na/fcc Ca, and E_G is the total energy of a particular graphene structure. We have computed the equilibrium energy for Na and Ca as −1.307 and −1.980 eV, respectively. If the energies are expressed in electron volts, then the potential of the structures versus Na/Na^+ as a function of Na content (and vs Ca/Ca^{2+} as a function of Ca content) can be obtained as[43]

$$V = -\frac{\Delta E}{n} \tag{4}$$

The composition range over which Na/Ca can be reversibly intercalated determines the battery's capacity.

RESULTS AND DISCUSSION

First, we discuss the defective graphene systems that we investigated for sodiation and calciation. Single vacancies (SV) with a carbon atom missing in graphene (or in the outermost layer of graphite) have been experimentally observed using TEM[33,44] and STM.[35] However, Meyer et al.[33] showed that SV undergoes a Jahn−Teller distortion, which leads to the saturation of two of the three dangling bonds toward the missing atom. For reasons of geometry, one dangling bond always remains. The SV appears as a protrusion in STM images because of an increase in the local density of states at the Fermi energy, which is spatially localized on the dangling bonds.[35] It is intuitively clear that the formation energy of such a defect is high because of the presence of an undercoordinated carbon atom. Hence, instead of SV defects, we have concentrated on DV defects, where no dangling bond is present. The atomic network remains coherent with minor perturbations in the bond lengths around the defect. Simulations[45,46] indicate that the formation energy, E_f, of a DV is of the same order as for an SV (about 8 eV). As two atoms are now missing, the energy per missing atom (4 eV per atom) is much lower than for an SV. Hence, a DV is thermodynamically favored over an SV. Moreover, DV defects are the most common type of vacancy defects observed experimentally,[47,48] and as mentioned before, structures with any other kind of vacancy defect with dangling bonds are not stable.[49] As shown in Figure 1, a DV defect can be obtained by removing C−C dimers from pristine graphene.

dx.doi.org/10.1021/am404788e | ACS Appl. Mater. Interfaces XXXX, XXX, XXX−XXX

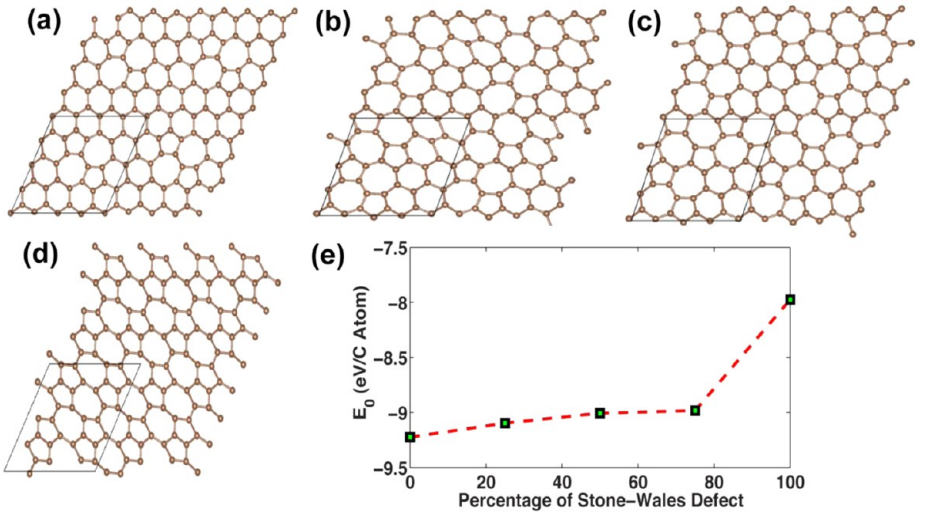

Figure 2. Graphene with SW defects: (a) 25, (b) 50, (c) 75, and (d) 100%. Systems shown here are 2 × 2 in size with periodicity in their in-plane dimensions. The super cell used in the calculation is marked in black. All systems are relaxed structure. (e) Equilibrium energy per carbon atom for different percentages of SW defect.

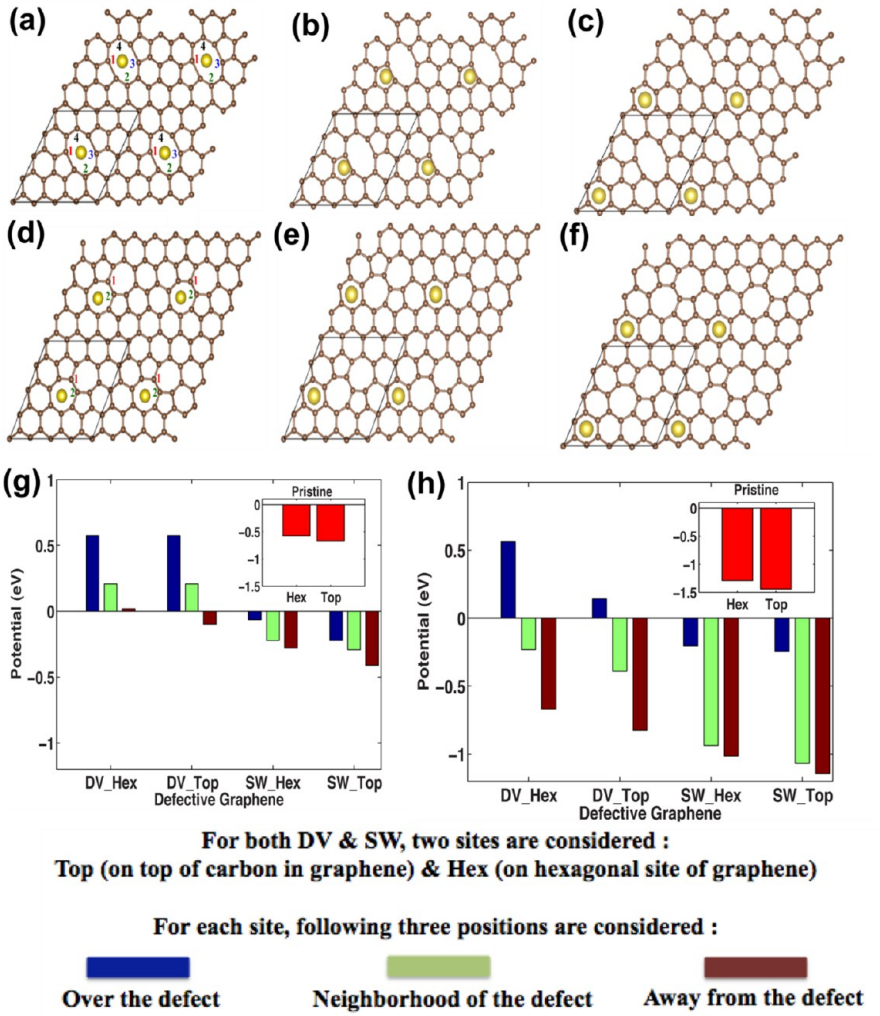

Figure 3. Na adsorption on graphene with (a–c) 6.25% DV defect and (d–f) 25% SW defect: adatom (a, d) over the defect (O position), (b, e) neighborhood of defect (N position), and (c, f) away from defect (A position). (g) Sodiation and (h) calciation potential for Na/Ca adsorption on different locations: pristine graphene (inset) and graphene with DV and SW defects at the Hex and Top sites. For each site, three positions, O (blue), N (green), and A (brown), are shown. Location 1 (a, d) is the Top site at the O position.

dx.doi.org/10.1021/am404788e | ACS Appl. Mater. Interfaces XXXX, XXX, XXX–XXX

Table 1. Sodiation and Calciation Potential (V in eV) for Different Positions of Adatom at Different Sites in Defective Graphene

defect		DV						SW					
site		Hex			Top			Hex			Top		
positions		O	N	A	O	N	A	O	N	A	O	N	A
V in eV	Na	0.574	0.207	0.019	0.574	0.207	−0. 098	−0.063	−0.221	−0.278	−0.221	−0.292	−0.410
	Ca	0.562	−0.231	−0.671	0.142	−0.391	−0. 824	−0.204	−0.937	−1.016	−0.243	−1.069	−1.14

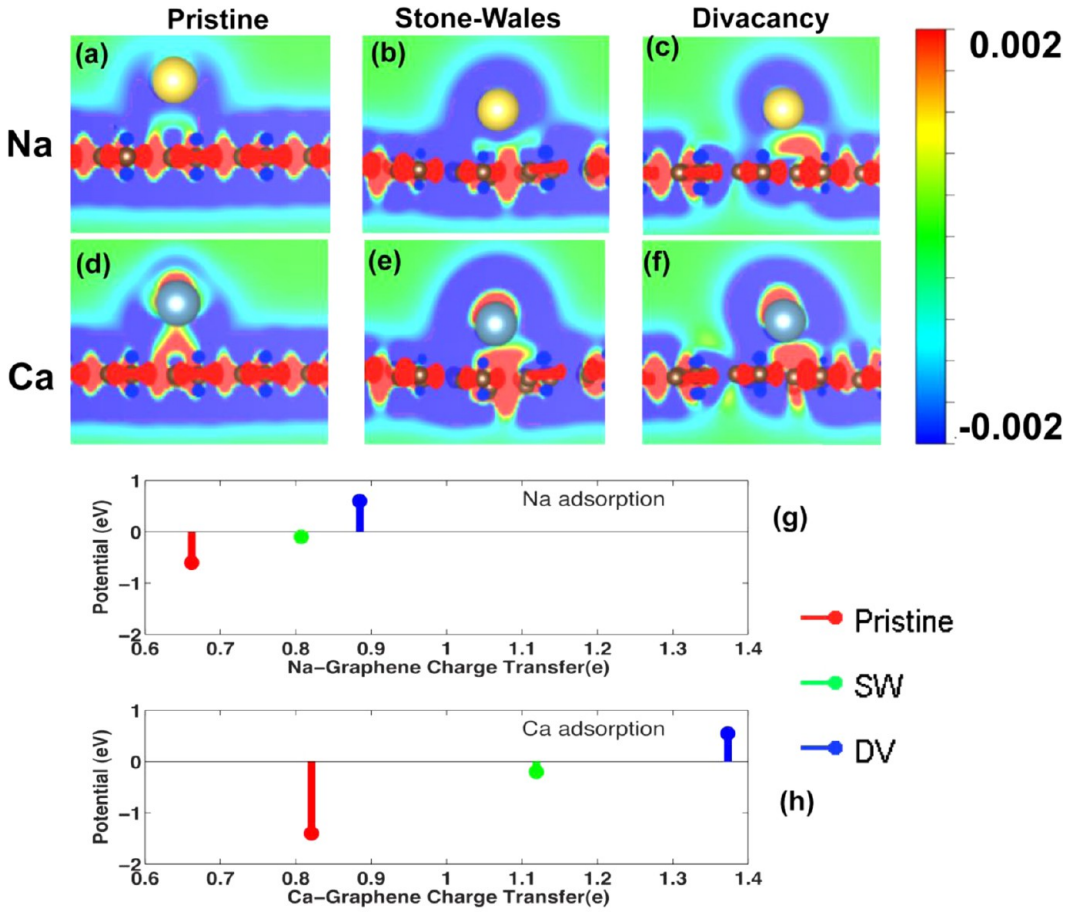

Figure 4. Bonding charge density for Na and Ca (Top site and O position) for (a, d) pristine, (b, e) Stone−Wales, and (c, f) divacancy systems obtained as the charge-density difference between the valence charge density before and after the bonding. Red and blue colors indicate the electron accumulation and depletion, respectively. The color scale is in the units of e/Bohr.[3] Potential vs charge transfer for (g) Na and (h) Ca adsorption.

Five different percentages of defects are considered here: 6.25 (Figure 1b), 12.50 (Figure 1c), 16.00 (Figure 1d), 18.75 (Figure 1e), and 25% (Figure 1f). All of the systems shown here are relaxed structures. Figure 1g shows that numerical value of equilibrium energy (i.e., the total ground-state energy per carbon atom) gradually decreases with the increase in DV defects.

Like DV, SW defects are another common type of structural defect observed experimentally.[50] The SW (55−77) defect has a formation energy E_f = 5 eV.[50] The defective structure retains the same number of atoms as pristine graphene, and no dangling bonds are introduced. As shown in Figure 2, we have considered four types of SW defects with different defect concentration: 25 (Figure 2a), 50 (Figure 2b), 75 (Figure 2c), and 100% (Figure 2d). For 100% SW defect, we have the Haeckelite structure,[51] which is a sheet full of 5−7 rings. The equilibrium energy per carbon atom is much less in this configuration (Figure 2e).

We first focus on pristine and lowest defect density. The lattice constant of graphene is 2.46 Å.[52,53] We consider two sites of high symmetry for adsorption: the site on the top of a carbon atom (Top) and the site at the center of a hexagon (Hex) of a graphene sheet. The inset in Figure 3, panels g and h (in red) shows the sodiation and calciation potential for pristine graphene, respectively. The negative potential indicates that adsorption is not possible. Next, we investigate the influence of the lowest defect density: 6.25% DV defect and 25% SW defect. For both Hex and Top sites, we consider three positions: over the defect (O position), neighborhood of the defect (N position), and away from the defect (A position). Figure 3, panels a−c and d−f show Na on the O (Figure 3a,d), N (Figure 3b,e), and A (Figure 3c,f) positions at the Hex site of graphene with a DV defect and SW defect, respectively. Here, defect location considers the defect with maximum intensity. For example, one may claim the site over the five-carbon ring in Figure 3a as being over the defect. However, the site over the

dx.doi.org/10.1021/am404788e | ACS Appl. Mater. Interfaces XXXX, XXX, XXX−XXX

eight-carbon ring refers to maximum defect intensity. Similarly, we consider the O, N, and A positions at the Top site.

In describing the Top site at the O position, we have a couple of options for the case of the DV defect. As shown in Figure 3a, we can place adatom in any of the eight carbons enclosing the octagon. However, carbon at locations 1 and 3 has the same neighborhood as well as for carbon at locations 2 and 4. Similarly, carbon in between 1 and 2 has the same surrounding as it does between 3 and 4. Hence, we conclude that we have only two different options (locations 1 and 2). Between these two locations, we select the location that has the maximum defective neighborhood (MDN). Location 1 is at the junction of an octagon, hexagon, and pentagon, whereas for location 2, it is at the junction of an octagon and two hexagons. Hence, we select location 1, which has the MDN. However, for graphene with Stone−Wale defect, as shown in Figure 3d, both locations 1 and 2 have the same neighborhood (i.e., they are identical). Hence, we select location 1.

The sodiation and calciation potentials for three different positions (O, N, and A) for both the Hex and Top sites are summarized in Table 1. The information in Table 1 is condensed in Figure 3, panels g (sodiation potential) and h (calciation potential). For DV_Hex (Hex site of DV defect) and DV_Top (Top site of DV defect), we notice that the O position (blue), as expected, is the most favorable position for adsorption. Sodiation potential is reduced to zero or is negative from the O to A positions. For the SW defect, the lowest defect density (25%) does not favor Na adsorption for any location. However, the O position has a less negative potential compared to the N and A positions. The same procedure applies for the calculations for Ca, and a similar trend is obtained, as shown in Figure 3h. It is clear that adatoms tend to cluster around the defective zone.

To obtain insight on the adsorption on defective sheets, we performed bonding charge-density analysis.[54] Figure 4 shows the bonding charge-density passing through the bond between Na/Ca and the nearest carbon atom. The bonding charge density is obtained as the difference between the valence charge density of strain-free graphene-Na/Ca sheet and the superposition of the valence charge density of the constituent atoms. A positive value (red) indicates electron accumulation, whereas a negative value (blue) denotes electron depletion. These changes in bonding charge distributions after introduction of defects clearly show that the enhanced charge transfer from Na/Ca to graphene sheet leads to adsorption of adatoms.

The charge redistribution can be quantitatively estimated by computing the charge transfer using Bader charge analysis. Table 2 shows the magnitude of the charge transfer for different positions. In case of the Na^+ ion, charge transfer to pristine graphene is 0.6617*e*, whereas for structures with DV and SW defects, the transferred charges are increased to 0.8848*e* and 0.8073*e*, respectively. For Ca^{2+}, the corresponding charge transfer is 0.8208*e*, 1.3727*e*, and 1.1189*e*, respectively. For each case, the DV defect case has more charge transfer, resulting in more adsorption of adatoms. In Figure 4g,h, for both Na and Ca adsorption, the potential increases with the increase in charge transfer. Any amount of charge transfer does not imply adsorption. There is a threshold of charge transfer beyond which adsorption is possible. Depending on the adatom (i.e., Na/Ca in this study), the threshold is different. From Figure 4g,h, we can observe that charge transfer over 0.85*e* (approximately) favors Na adsorption, whereas for Ca, the corresponding threshold is around 1.30*e*.

Table 2. Charge Transfer from Na/Ca to Graphene

ion	pristine	divacancy	Stone−Wales
Na^+	0.6617*e*	0.8848*e*	0.8073*e*
Ca^{2+}	0.8208*e*	1.3727*e*	1.1189*e*

From our results in Figures 3 and 4, we have discovered that the O position of the Hex site is the most favorable location of adsorption. Hence, we primarily focus on this location while initially distributing the Na/Ca adatoms. Still, for every case, there are many possibilities of initial distribution. For each case, we have considered three different initial configurations to obtain the potential range, and we reported the average values. It is obvious that at low concentration a greater possibility of initial distribution leads to a wider range of potential. For each percentage of defects, we have carried out DFT calculations for different Na/Ca concentrations until we crossed the maximum limit of capacity (i.e., when the potential becomes negative).

Figure 5a summarizes the sodiation potential for five different DV defect percentages. For each defect density, the potential decreases with the increase in the Na concentration. For higher defect density, the potential is larger for a given Na concentration and the maximum percentage of adsorbed Na is increased. As shown in Figure 1f, 25% is the maximum DV defect density possible. Beyond this limit, the structure will have dangling bonds.[49] Figure 5b shows one of the configurations of Na_8C_{26} where Na adatoms are mainly located on and around O positions (i.e., adatoms tend to cluster around the defective zone). As shown in Figure 5c, for SW defects, the percentage of adsorption is increased with the increase in defect density. Figure 5d shows one of the configurations of Na_6C_{32}. The results for calcium adsorption are summarized in Figure 6. We note that the adsorption behavior of Ca in DV and SW graphene is qualitatively the same as for Na.

Figure 7 summarizes the maximum percentage of Na/Ca adsorbed for different percentages of DV and SW defects. Capacity, *C* (mAh/g), can be computed from percentage of adsorption, *p*, as

$$C = \frac{1}{A_c}\left[\left(\frac{p}{100}\right)vF10^3\right] \tag{5}$$

Where *p* is the percentage of adsorption of adatoms on graphene (%), *v* is the vacancy (Na = 1; Ca = 2), *F* is the Faraday constant (26.801 Ah/mole), and A_c is the atomic mass of Carbon (12.011)

For the 6.25% DV defect, the maximum percentage of adsorption is 6.67%, corresponding to a capacity of 148.8325 mAh/g for Na and 297.6649 mAh/g for Ca. With the increase in defect density, we obtained a maximum percentage of adsorption for Na/Ca around 19, 25, 40, and 65% for 12.50, 16, 18.75, and 25% defects, respectively. Hence, for a maximum defect density of 25%, we can obtain a maximum capacity of around 1450 mAh/g for Na and 2900 mAh/g for Ca. For SW defects, the maximum percentage of adsorption is around 10, 13, and 48% for 50, 75, and 100% of SW defects, respectively. Hence, for the 100% SW defect (i.e., structure full of 5−7 rings), we can achieve a maximum capacity of around 1071 and 2142 mAh/g for Na and Ca, respectively. We observe that for DV defects the capacity increases gradually with the increase of defect density. However, for SW defects, until the system reaches its maximum defect density (i.e., a system full of 5−7

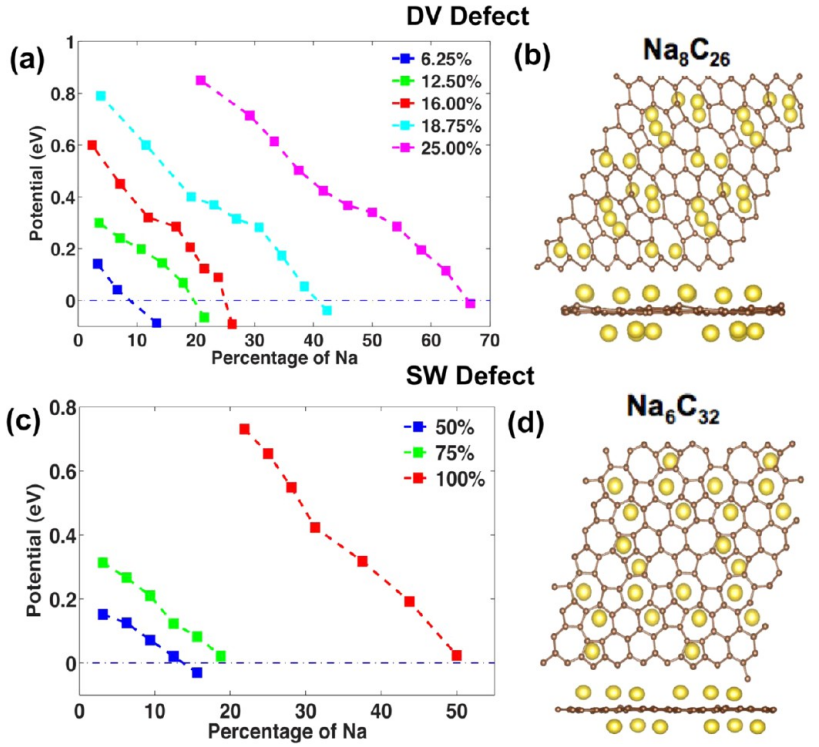

Figure 5. Sodiation potential for different percentages of Na adsorbed for different percentages of (a) DV and (c) SW defects. Top and side view of one of the (b) Na_8C_{26} and (d) Na_6C_{32} relaxed configurations.

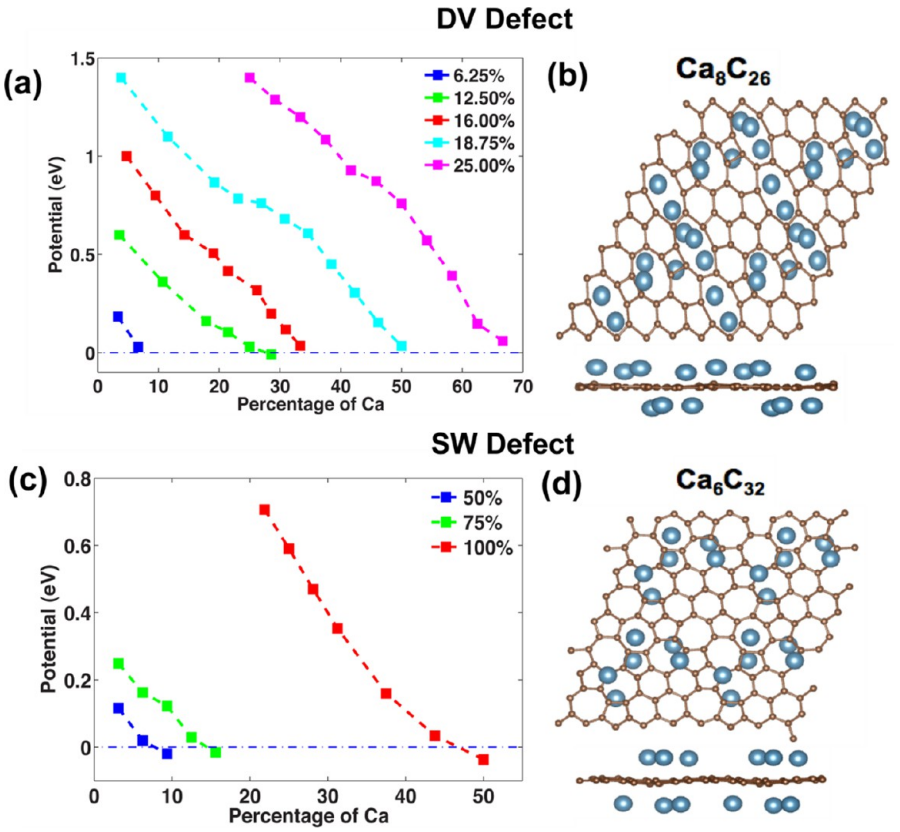

Figure 6. Calciation potential for different percentages of Ca adsorbed for different percentages of (a) DV and (c) SW defects. Top and side view of one of the (b) Ca_8C_{26} and (d) Ca_6C_{32} relaxed configurations.

rings), the capacity does not increase much. This can be attributed to the fact that for Haeckelite structure, the drop in equilibrium energy is drastic, whereas for DV defects, the drop in equilibrium energy is gradual.

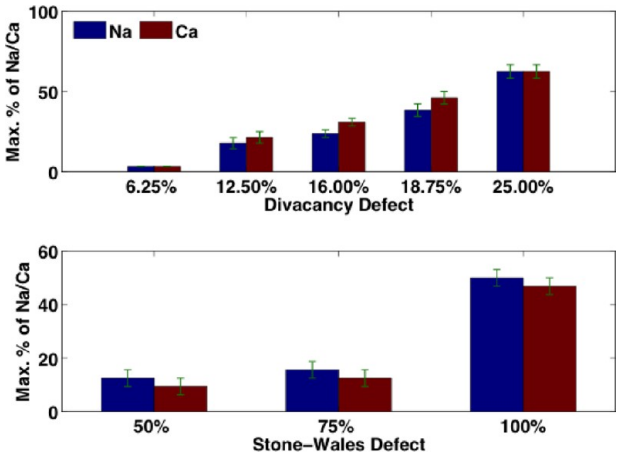

Figure 7. Maximum percentages of Na/Ca adsorbed for different percentages of DV and SW defects.

CONCLUSIONS

We have performed first-principles calculations to study the Na and Ca adsorption on graphene with various percentages of DV and SW defects. Our results show that adsorption is not possible in pristine graphene. However, the presence of defects enhances the adsorption, and the potential is larger when the adatoms are on and around the defective zone. With the increase in defect density, the maximum capacity obtained is much higher than that of graphite. This study will help to create better anode materials that can replace graphite for higher capacity and better cycling performance NIBs and CIBs. It will be interesting to compare our results with future experiments.

AUTHOR INFORMATION

Corresponding Author

*E-mail: vshenoy@seas.upenn.edu.

Notes

The authors declare no competing financial interest.

ACKNOWLEDGMENTS

D.D., J.L., and V.B.S. gratefully acknowledge the support of the Army Research Office through contract W911NF-11-1-0171 and the National Science Foundation.

REFERENCES

(1) Dahn, J. R.; Zheng, T.; Liu, Y. H.; Xue, J. S. *Science* **1995**, *270*, 590.
(2) Armand, M.; Tarascon, J. M. *Nature* **2008**, *451*, 652.
(3) Dunn, B.; Kamath, H.; Tarascon, J. M. *Science* **2011**, *334*, 928.
(4) Whittingham, M. S. *Science* **1976**, *192*, 1226.
(5) Tarascon, J. M.; Armand, M. *Nature* **2001**, *414*, 359.
(6) Teng, F. Z.; McDonough, W. F.; Rudnick, R. L.; Dalpé, C.; Tomascak, P. B.; Chappell, B. W.; Gao, S. *Geochim. Cosmochim. Acta* **2004**, *68*, 4167.
(7) Palomares, V.; Serras, P.; Villaluenga, I.; Hueso, K. B.; Carretero-González, J.; Rojo, T. *Energy Environ. Sci.* **2012**, *5*, 5884.
(8) Ong, S. P.; Chevrier, V. L.; Hautier, G.; Jain, A.; Moore, C.; Kim, S.; Ma, X. H.; Ceder, G. *Energy Environ. Sci.* **2011**, *4*, 3680.
(9) Kim, S.-W.; Seo, D.-H.; Ma, X.; Ceder, G.; Kang, K. *Adv. Energy Mater.* **2012**, *2*, 710.
(10) Hayashi, M.; Arai, H.; Ohtsuka, H.; Sakurai, Y. *J. Power Sources* **2003**, *119*, 617.
(11) Amatucci, G. G.; Badway, F.; Singhal, A.; Beaudoin, B.; Skandan, G.; Bowmer, T.; Plitza, I.; Pereira, N.; Chapman, T.; Jaworski, R. *J. Electrochem. Soc.* **2001**, *148*, 940.
(12) Lin, Y. M.; Abel, P. R.; Gupta, A.; Goodenough, J. B.; Heller, A.; Mullins, C. B. *ACS Appl. Mater. Interfaces* **2013**, *5*, 8273.
(13) Seyfried, W. E.; Janecky, D. R.; Mottl, M. J. *Geochim. Cosmochim. Acta* **1984**, *48*, 557.
(14) Liu, J.; Zhang, J. G.; Yang, Z. G.; Lemmon, J. P.; Imhoff, C.; Graff, G. L.; Li, L. Y.; Hu, J. Z.; Wang, C. M.; Xiao, J.; Xia, G.; Viswanathan, V. V.; Baskaran, S.; Sprenkle, V.; Li, X. L.; Shao, Y. Y.; Schwenzer, B. *Adv. Funct. Mater.* **2013**, *23*, 929.
(15) Mortazavi, M.; Deng, J. K.; Shenoy, V. B.; Medhekar, N. V. *J. Power Sources* **2013**, *225*, 207.
(16) Zhu, H.; Jia, Z.; Chen, Y.; Weadock, N.; Wan, J.; Vaaland, O.; Han, X.; Li, T.; Hu, L. *Nano Lett.* **2013**, *13*, 3093.
(17) Rogosic, J.; Sadoway, D. R. Pacific Rim Meeting on Electrochemical and Solid-State Science (PRIME), Honululu, HI, Oct 7–12, 2012; 664.
(18) Xu, J.; Lavan, D. A. *Nat. Nanotechnol.* **2008**, *3*, 666.
(19) Divincenzo, D. P.; Mele, E. J. *Phys. Rev. B* **1985**, *32*, 2538.
(20) Medeiros, P. V. C.; Mota, F. D.; Mascarenhas, A. J. S.; de Castilho, C. M. C. *Nanotechnology* **2010**, *21*, 115701.
(21) Ataca, C.; Akturk, E.; Ciraci, S.; Ustunel, H. *Appl. Phys. Lett.* **2008**, *93*, 043123.
(22) Stournara, M. E.; Shenoy, V. B. *J. Power Sources* **2011**, *196*, 5697.
(23) Shimoda, H.; Gao, B.; Tang, X. P.; Kleinhammes, A.; Fleming, L.; Wu, Y.; Zhou, O. *Phys. Rev. Lett.* **2002**, *88*, 015502.
(24) Meunier, V.; Kephart, J.; Roland, C.; Bernholc, J. *Phys. Rev. Lett.* **2002**, *88*, 075506.
(25) Chan, C. K.; Peng, H. L.; Liu, G.; McIlwrath, K.; Zhang, X. F.; Huggins, R. A.; Cui, Y. *Nat. Nanotechnol.* **2008**, *3*, 31.
(26) Novoselov, K. S.; Geim, A. K.; Morozov, S. V.; Jiang, D.; Zhang, Y.; Dubonos, S. V.; Grigorieva, I. V.; Firsov, A. A. *Science* **2004**, *306*, 666.
(27) Lv, W.; Tang, D. M.; He, Y. B.; You, C. H.; Shi, Z. Q.; Chen, X. C.; Chen, C. M.; Hou, P. X.; Liu, C.; Yang, Q. H. *ACS Nano* **2009**, *3*, 3730.
(28) Yoo, E.; Kim, J.; Hosono, E.; Zhou, H.; Kudo, T.; Honma, I. *Nano Lett.* **2008**, *8*, 2277.
(29) Jang, B. Z.; Liu, C. G.; Neff, D.; Yu, Z. N.; Wang, M. C.; Xiong, W.; Zhamu, A. *Nano Lett.* **2011**, *11*, 3785.
(30) Banhart, F.; Kotakoski, J.; Krasheninnikov, A. V. *ACS Nano* **2011**, *5*, 26.
(31) Hashimoto, A.; Suenaga, K.; Gloter, A.; Urita, K.; Iijima, S. *Nature* **2004**, *430*, 870.
(32) Terrones, H.; Lv, R.; Terrones, M.; Dresselhaus, M. S. *Rep. Prog. Phys.* **2012**, *75*, 062501.
(33) Meyer, J. C.; Kisielowski, C.; Erni, R.; Rossell, M. D.; Crommie, M. F.; Zettl, A. *Nano Lett.* **2008**, *8*, 3582.
(34) Kotakoski, J.; Krasheninnikov, A. V.; Kaiser, U.; Meyer, J. C. *Phys. Rev. Lett.* **2011**, *106*, 105505.
(35) Ugeda, M. M.; Brihuega, I.; Guinea, F.; Gomez-Rodriguez, J. M. *Phys. Rev. Lett.* **2010**, *104*, 096804.
(36) Ugeda, M. M.; Brihuega, I.; Hiebel, F.; Mallet, P.; Veuillen, J. Y.; Gomez-Rodriguez, J. M.; Yndurain, F. *Phys. Rev. B* **2012**, *85*, 121402.
(37) Zhou, L.-J.; Hou., Z. F.; Wu., L.-M. *J. Phys. Chem. C* **2012**, *116*, 21780.
(38) Liu, Y. Y.; Artyukhov, V. I.; Liu, M. J.; Harutyunyan, A. R.; Yakobson, B. I. *J. Phys. Chem. Lett.* **2013**, *4*, 1737.
(39) Kresse, G.; Furthmuller, J. *Phys. Rev. B* **1996**, *54*, 11169.
(40) Kresse, G.; Joubert, D. *Phys. Rev. B* **1999**, *59*, 1758.
(41) Blochl, P. E. *Phys. Rev. B: Condens. Matter Mater. Phys.* **1994**, *50*, 17953.
(42) Perdew, J. P.; Burke, K.; Wang, Y. *Phys. Rev. B* **1996**, *54*, 16533.
(43) Aydinol, M. K.; Ceder, G. *J. Electrochem. Soc.* **1997**, *144*, 3832.
(44) Gass, M. H.; Bangert, U.; Bleloch, A. L.; Wang, P.; Nair, R. R.; Geim, A. K. *Nat. Nanotechnol.* **2008**, *3*, 676.
(45) Krasheninnikov, A. V.; Lehtinen, P. O.; Foster, A. S.; Nieminen, R. M. *Chem. Phys. Lett.* **2006**, *418*, 132.
(46) El-Barbary, A. A.; Telling, R. H.; Ewels, C. P.; Heggie, M. I.; Briddon, P. R. *Phys. Rev. B* **2003**, *68*, 144107.

(47) Lahiri, J.; Lin, Y.; Bozkurt, P.; Oleynik, I. I.; Batzill, M. *Nat. Nanotechnol.* **2010**, *5*, 326.
(48) Carlsson, J. M.; Scheffler, M. *Phys. Rev. Lett.* **2006**, *96*, 046806.
(49) Brunetto, G.; Autreto, P. A. S.; Machado, L. D.; Santos, B. I.; dos Santos, R. P. B.; Galvao, D. S. *J. Phys. Chem. C* **2012**, *116*, 12810.
(50) Li, L.; Reich, S.; Robertson, J. *Phys. Rev. B* **2005**, *72*, 165423.
(51) Terrones, H.; Terrones, M.; Hernandez, E.; Grobert, N.; Charlier, J. C.; Ajayan, P. M. *Phys. Rev. Lett.* **2000**, *84*, 1716.
(52) Fan, X. F.; Zheng, W. T.; Kuo, J. L. *ACS Appl. Mater. Interfaces* **2012**, *4*, 2432.
(53) Yang, C.-K. *Appl. Phys. Lett.* **2009**, *94*, 163115.
(54) Li, J.; Medhekar, N. V.; Shenoy, V. B. *J. Phys. Chem. C* **2013**, *117*, 15842.